*J Genet Resour 2026; 12(2): 116-130* *Homepage: http://sc.journals.umz.ac.ir/*

**RESEARCH ARTICLE** *DOI: 10.22080/jgr.2026.32150.1473*

J|G|R

# A Mineral Paper-based Scaffold as a Platform for Osteogenic Differentiation

Mina Amiryousefi, Mahdie Matin, Naser Farrokhi, Mayda Sharei
Hosein Shahsavarani* and Shirin Farivar*

Department of Cell and Molecular Biology, Faculty of Life Sciences and Biotechnology, Shahid Beheshti University, Tehran, Iran

**ARTICLE INFO**

***Article history:***
Received 28 May 2026
Accepted 22 June 2026
Available 12 July 2026

***Keywords:***
Bone
Mesenchymal stem cell
Mineral paper
Tissue engineering
Transcript analysis

***Corresponding authors:***
✉ H. Shahsavarani
h_shahsavarani@sbu.ac.ir
✉ S. Farivar
s_farivar@sbu.ac.ir

p-ISSN 2423-4257
e-ISSN 2588-2589

**ABSTRACT**

Despite tissue engineering's promise for critical-sized bone defects and nonunions, most current approaches rely heavily on complex growth factors and elaborate composites. In contrast to such multifaceted strategies, we examined a mineral paper scaffold composed of HDPE and calcium carbonate and cultured adipose-derived mesenchymal stem cells on it without exogenous osteogenic inducers. The scaffold's surface showed microscale roughness and hydrophilic behavior, and its degradation proceeded steadily over 62 days. FTIR and XRD confirmed the calcium carbonate as calcite. Flow cytometry initially confirmed the mesenchymal phenotype of the adipose-derived cells (high CD90, CD105, CD29 vs. low CD34, CD45). During subsequent culture on the scaffold, the scaffold itself not only supported a steady rise in cell metabolism but, more critically, induced osteogenic differentiation. Alkaline phosphatase activity on the scaffold significantly exceeded that on standard tissue culture plate controls on days 7 and 14. RUNX2 and BGLAP expression were also elevated in cells cultured on the mineral paper relative to controls by day 14. We attribute the osteogenic response to the scaffold's surface topography, which appears sufficient for guiding ADSC osteoinductivity in the absence of soluble inducers. These findings support the use of mineral paper as a structurally driven, low-complexity scaffold for bone tissue engineering and human bone regeneration.



***Please cite this paper as:*** Amiryousefi, M., Matin, M., Farrokhi, N., Sharei, M., Shahsavarani, H., & Farivar, SH. (2026). A mineralized paper-based scaffold as a platform for osteogenic differentiation. *Journal of Genetic Resources*, 12(2), 116-130. doi: 10.22080/jgr.2026.32150.1473

## Introduction

Bone defects constitute one of the most complex challenges in contemporary orthopedics and regenerative medicine (De Pace *et al.*, 2025; Zhang *et al.*, 2020). Bone defects may adversely affect both shape and biological functionality, leading to pain, disabilities, reduced life quality, and predisposition to further bone injuries (Ciancia *et al.*, 2022). Although bone tissue has an intrinsic capacity for regeneration, this ability is often insufficient in critical-sized defects and nonunion, where clinical intervention is required (Schulze *et al.*, 2023). Therefore, the restoration of biological activity and functional properties of bone is among the research and development priorities (Duda *et al.*, 2023). Current strategies for bone regeneration include autografts, allografts, xenografts, synthetic bone substitutes, naturally derived biomaterials, and scaffold-based tissue engineering approaches (Battafarano *et al.*, 2021; Qi *et al.*, 2021). Autografts are acknowledged as the gold standard due to their biological compatibility and regenerative potential (Ferraz, 2023). However, donor-site morbidity, lack of graft material, infections, risk of fractures, necessity for additional surgery, and high costs are considered its shortcomings. Looking into other graft materials is therefore required (Younger and Chapman, 1989). The use of allografts and xenografts partially solves the problem of tissue availability, although questions

about the safety, integration, and effectiveness of such tissues should not be overlooked (Hakami, 2024; Kotsifaki *et al.*, 2025). Bone tissue engineering is an alternative in addressing the above issues, using biomaterials, living cells, and bioactive factors incorporated in scaffold systems (Ferraz, 2024). atrix formation during bone regeneration (Xu *et al.*, 2017; Hajihassani *et al.*, 2026). A wide range of scaffold systems, including polymeric (Liu and Ma, 2004), ceramic (Wen *et al.*, 2017), metallic (Alvarez and Nakajima, 2009), hydrogel (Liu *et al.*, 2023), fibrous (Moy *et al.*, 2020), and composite (Wang, 2006), have been used for bone tissue engineering purposes (Donnaloja *et al.*, 2020; Farjaminejad *et al.*, 2024; Filippi *et al.*, 2020). Calcium-based biomaterials, mimics of the inorganic bone component, play a significant role in bone tissue engineering (Min *et al.*, 2024; Ribas *et al.*, 2019). Calcium phosphate- (Jeong *et al.*, 2019) and calcium carbonate-based (Chernozem *et al.*, 2019; Kajander *et al.*, 2023) materials have been widely used due to their chemical similarity to the mineral phase of bone and teeth, as well as their favorable biocompatibility and osteoconductivity. Beyond their structural role, calcium-containing substrates may also influence osteogenic differentiation through chemical and physical cues. Calcium-rich surfaces can contribute to a local ionic microenvironment that may affect calcium-sensitive signaling pathways, while surface roughness and micro-topography can regulate cell adhesion, cytoskeletal organization, mechanotransduction, and downstream osteogenic gene expression. These platforms, *i.e.*, calcium-based paper-like scaffolds, offer low cost, high porosity, ease of handling, flexibility in processing and formability, and improved oxygen diffusion compared to bulk 3D scaffolds, attracting attention in bone tissue engineering. Traditional paper substrates, however, suffer from relatively low tensile strength, particularly when moistened, making it impractical for weight-bearing structures. Mineral paper, also known as stone paper, is a synthetic paper-like substrate mainly composed of calcium carbonate and a small fraction of high-density polyethylene (HDPE) (Chu and Nel, 2019). Traditional calcium-based scaffolds often require sophisticated fabrication techniques with high production costs. Mineral paper presents a unique, cost-effective, and ready-to-use composite platform. The presence of HDPE provides mechanical flexibility and structural stability, unlike brittle ceramic scaffolds. However, as a polymeric component, HDPE may also affect surface wettability and initial cell adhesion; therefore, its possible interference with cell attachment and spreading should be evaluated through cell adhesion, viability, and morphology assessments. At the same time, the $CaCO_3$-rich phase and the HDPE/$CaCO_3$ composite surface may provide mineral and topographical cues that influence cell-material interactions and osteogenic commitment. Despite the widespread use of calcium carbonate in bone tissue engineering, the potential of this specific industrial material to serve as an osteoconductive and supportive platform for mesenchymal stem cells remains unexplored. This study addresses the knowledge gap regarding whether the intrinsic mineral cues and surface properties of this industrial material can independently support osteogenic differentiation without the need for exogenous osteogenic supplements. The present study investigates a calcium carbonate-rich mineral paper-based scaffold as a platform for osteogenic differentiation.

## Materials and Methods

### Materials

Mineral paper, composed primarily of calcium carbonate ($CaCO_3$) and high-density polyethylene (HDPE), was obtained from Azarakhs Sanaat Pouyapars Co, Iran, and employed as the scaffold. Dulbecco's Modified Eagle Medium/Nutrient Mixture F-12 (DMEM/F12), fetal bovine serum (FBS), collagenase type I, phosphate-buffered saline (PBS), and TRIzol reagent were obtained from Gibco (New York, NY, USA). Penicillin-streptomycin solution and Trypsin-EDTA were purchased from BioIdea (Iran). The cDNA synthesis kit and SYBR Green qPCR master mix were obtained from Pars-Tous Biotechnology (Iran). Primary antibodies against CD29, CD90, CD105, CD34, and CD45 and their corresponding secondary antibodies were used for flow cytometric characterization of ADSCs. Resazurin sodium salt was purchased from Sigma-Aldrich (St. Louis, MO, USA) and was used for cell viability assessment, and a commercial alkaline

phosphatase (ALP) assay kit was obtained from Pars Azmoon (Tehran, Iran).

**Scaffold surface analysis**

Circular scaffold samples with a diameter of approximately 10 mm were prepared, washed with $dH_2O$, and air-dried before analysis. To improve surface conductivity and minimize charging effects during imaging, the samples were sputter-coated with a thin layer of gold. Surface morphology was examined using a SU3500 scanning electron microscope (Hitachi High-Tech Corporation, Tokyo, Japan) operating in secondary electron (SE) mode at an accelerating voltage of 15 kV. The surface topography and roughness of the scaffolds were evaluated using atomic force microscopy (AFM) at the Laser Research Institute, Shahid Beheshti University. AFM analysis was performed using an Easyscan 2 atomic force microscope (Nanosurf AG, Liestal, Switzerland). To identify the main functional groups and chemical components, the scaffold was ground into powder before FTIR analysis in the 4000- 400 $cm^{-1}$ spectral range. X-ray diffraction (XRD) was used to evaluate the crystallinity of the scaffold samples. The scaffold samples were first ground into powder and analyzed using a STOE Theta-Theta diffractometer (STOE & Cie GmbH, Darmstadt, Germany) equipped with Cu Kα radiation (λ = 1.5406 Å) and a scintillation counter detector. Measurements were performed in reflection mode over a 2θ range of 10° to 80°. The diffraction patterns were recorded and compared with standard reference patterns to identify the crystalline phases present in the scaffold and evaluate its crystallinity.

**Scaffold wettability**

Static water contact angle (WC) was employed to evaluate the surface wettability of three-dimensional scaffolds. Scaffolds were cut into sheets before experimentation, rinsed with $dH_2O$, and allowed to air-dry. A micro syringe was used to place $dH_2O$ (3-5 µl) on the scaffold surface. Images of the water droplet were acquired immediately after placing the water droplet on the scaffold using an optical microscope and analysis Contact Angle OCR software (version 1.10) to record the static contact angle. For each scaffold sample, static WC was measured from three different positions on the sheet.

***In vitro* scaffold degradation analysis**

For the investigation of scaffold degradation, the dry weight of samples was measured before incubation ($W_0$). The scaffolds were transferred into 24-well plates, and PBS solution (8 g/l NaCl, 0.2 g/l KCl, 1.44 g/l $Na_2HPO_4$, and 0.245 g/l $KH_2PO_4$) was added to each well. The samples were incubated at 37°C throughout the experiment. At predetermined time intervals (days 7, 14, 21, 28, 35, 42, 49, 56, and 62), scaffold samples were removed from the PBS solution, gently washed three times with $dH_2O$ to remove residual salts, and dried in an oven at 30°C until a constant weight was achieved. The final dry weight of the samples ($W_1$) was measured. The degradation percentage of scaffold samples was determined using the following equation:

Degradation percentage of scaffold= $([W_0 - W_1] / W_0) \times 100$.

**Cell isolation from human adipose tissue**

Samples of human adipose tissues were generously donated by Nikan Gharb Hospital (Tehran, Iran). After taking the samples, tissues were immediately placed in 50 mL sterile tubes filled with PBS supplemented with 3% (w/v) penicillin-streptomycin (BioIdea, Iran). The guidelines provided by the National Center for Genetic Resources were followed in a Class II biosafety cabinet to wash off blood remains or any other contaminants. The adipose tissue samples were washed three times with DMEM containing 3% penicillin-streptomycin over a total period of 15 min. After washing, tissues were cut into smaller pieces using a sterile surgical blade in a Petri dish. Visible connective and vascular tissues were removed. The tissue fragments were washed three times under the same conditions and incubated in collagenase type I solution (0.02 mg/ml; Gibco, USA) at 37°C for 45 min in a shaking incubator to digest the extracellular matrix and release the cells. Culture medium supplemented with 10% fetal bovine serum (FBS; Gibco, USA) was added to stop collagenase activity. The obtained cell suspension was centrifuged at 2000 rpm for 5 min. Following centrifugation, the upper lipid layer without cells

was discarded, and the pellet containing mesenchymal stem cells (MSCs) was collected carefully. The isolated cells were cultured in T-flasks containing complete culture medium composed of DMEM/F12 (Capricorn Scientific, Germany), L-glutamine, HEPES (15 mM), 10% FBS, and 1% penicillin-streptomycin (BioIdea, Iran). Cell cultures were maintained at 37°C in a humidified atmosphere containing 5% $CO_2$. After 72 h, the culture medium was replaced to remove non-adherent cells, while adherent mesenchymal stem cells remained attached to the flask surface.

**Flow cytometry characterization of ADSCs**

The immunophenotype of adipose-derived mesenchymal stem cells (ADSCs) was evaluated by flow cytometry according to the minimal criteria proposed by the International Society for Cellular Therapy (ISCT). The cells were assessed for the presence of mesenchymal markers CD29, CD90, and CD105 and the absence or low expression of hematopoietic markers CD34 and CD45. Cells of the third passage were centrifuged at 1300 rpm for 5 min. The supernatant was removed, and the cell concentration was measured. Approximately $10^6$ cells were collected for flow cytometry. Cells were washed using 1 ml of PBS and centrifuged again at 1000 rpm for 5 min. The supernatant was removed, and the cells were mixed with 50 µl of staining solution containing a 1:1000 dilution of primary antibody per $10^6$ cells and incubated at 4°C in the dark for 30 min. The cells were washed with PBS and stained with secondary antibody in 100 µl of solution for 30 min at 4°C in the dark. The cells were washed with PBS containing 2% (w/v) BSA and analyzed by flow cytometry.

**Cell seeding on the scaffold**

After disinfection, the scaffolds were placed in 48-well plates. ADSCs were detached, counted, and resuspended in complete culture medium. A 30 µl cell suspension at a density of $10^6$ cells/ml (representing an initial seeding load of $3 \times 10^4$ cells per scaffold) was carefully seeded onto each scaffold. This concentrated volume was used to ensure maximal cell-material interaction and localized attachment. The plates were then incubated for 1 h at 37°C in a 5% $CO_2$ incubator to allow for initial cell adhesion. Following this period, 300 µl of complete culture medium (DMEM/F12, 10% FBS, and 1% penicillin-streptomycin) was added to each well. It should be noted that the reported seeding density refers to the initial cell load applied directly to the scaffold surface, rather than the final concentration in the total volume of the well. For morphological evaluation of cell–scaffold interactions, ADSC-seeded scaffolds were examined by SEM after 7 and 14 days of culture.

**Cell viability assay**

Cell viability was assessed using the resazurin assay. Metabolically active cells reduce blue resazurin to pink. On days 1, 3, and 7, the culture medium was removed, and the samples were washed with PBS. Diluted (1:10 in culture medium) resazurin solution (350 µl) was added to each well, and the plates were incubated for 3 h at 37°C in a humidified atmosphere with 5% $CO_2$. The solution (100 µl) from each well was transferred to a 96-well plate, and absorbance was measured at 570 nm with a reference wavelength of 600 nm.

**Alkaline phosphatase assay**

Alkaline phosphatase (ALP) activity was measured using a commercial alkaline phosphatase assay kit according to the manufacturer's instructions. Briefly, cells cultured on the scaffolds were lysed using RIPA buffer, and the lysates were centrifuged at 12,000 rpm for 12 min at 4°C. The supernatant was collected and incubated with the ALP substrate solution. Absorbance was measured at 405 nm using a microplate reader. ALP activity was calculated based on the standard curve provided with the kit and expressed as U/L.

**Transcript analysis**

RNA isolation was carried out using the TRIzol procedure. Cells were washed in PBS and harvested using Trypsin-EDTA (BioIdea, Iran). The solution was neutralized using complete medium supplemented with FBS. The harvested cells were lysed in TRIzol (1 ml), and 200 µl chloroform was added for phase separation. The aqueous phase containing RNA was isolated. RNA precipitation was performed using 600 µl 4°C isopropanol, after which RNA was washed in 75% ethanol, dried in an air chamber, and dissolved in RNase-free sterile water. The

concentration and purity of the extracted RNA were determined using a spectrophotometer (NanoDrop™, Thermo Fisher Scientific), and only samples with an $A_{260}/A_{280}$ ratio between 1.8 and 2.0 were used for further analysis. Additionally, RNA integrity was examined by 1% agarose gel electrophoresis. cDNA synthesis was performed using a commercial cDNA synthesis kit (Pars-Tous, Iran) according to the manufacturer's instructions.

The expression levels of osteogenic-related genes were evaluated using real-time quantitative PCR (qPCR) with a StepOne ABI Real-Time PCR System (Applied Biosystems, USA). Reactions were performed in 96-well plates using cDNA as the template, SYBR Green master mix, and gene-specific primers designed for *GAPDH*, *BGLAP*, and *RUNX2*. *GAPDH* was used as the reference gene for normalization. The primer sequences were used as follows: *GAPDH* forward, 5′-GACAGGCAACTTGGCAAATC-3′ and reverse, 5′-CCTTCTCAAGCCCCTCCTACA-3′; BGLAP forward, 5′-ACATCCTCGCCCTATTG-3′ and reverse, 5′-GATGTGGTCAGGCCAACTC-3′; *RUNX2* forward, 5′-GCCTTCAAGTGGTACCCC-3′ and reverse, 5′-CGTTACCCGCCATGAGAGTA-3′. The annealing temperatures for *GAPDH*, *BGLAP*, and *RUNX2* were 57.75°C, 60.18°C, and 58.54°C, respectively. The expected amplicon sizes were 111 bp for *GAPDH*, 133 bp for *BGLAP*, and 125 bp for *RUNX2*. The qPCR cycling protocol consisted of an initial denaturation step at 95°C for 30 s, followed by 40 cycles of [95°C: 5s; 57.75°C: 30s; 60.18°C and 58.54°C for *GAPDH*, *BGLAP*, and *RUNX2*: 30s, respectively]. A melt curve analysis was performed at the end of each run to verify amplification specificity. Fluorescence signals were recorded to determine Ct values, and relative gene expression levels were calculated using the $2^{-\Delta\Delta Ct}$ method (Livak and Schmittgen, 2001).

**Statistical analysis**

All experiments were conducted with at least three independent biological replicates (n= 3), each performed in technical triplicate to ensure reproducibility. Statistical analyses were performed using GraphPad Prism (GraphPad Software, Inc., USA). Data are presented as mean ± standard deviation (SD). Comparisons between two groups were performed using Student's t-test. In comparison, more than two groups were analyzed using one-way analysis of variance (ANOVA) followed by Tukey's post hoc test. A p-value< 0.05 was considered statistically significant.

**Results**

**Scaffold surface morphological analysis**

The micrographs showed a relatively compact and non-uniform surface morphology with limited visible porosity. Although the scaffold did not exhibit a highly interconnected porous architecture, small surface voids and irregularities were observed, which may contribute to surface-level cell attachment and limited diffusion of nutrients and oxygen. AFM analysis further confirmed the presence of micro-scale surface irregularities, with peak height values reaching approximately 1 µm (Fig. 1A and B)

**Chemical composition analysis of the scaffold**

The absorption bands observed at 711-877 $cm^{-1}$ and 1375-1407 $cm^{-1}$ correspond to characteristic vibrational modes of carbonate ions ($CO_3^{2-}$), confirming the presence of calcium carbonate in the scaffold. Moreover, the absorption bands at 2848-2952 $cm^{-1}$ are attributed to C-H stretching vibrations of methyl and methylene groups, consistent with the presence of high-density polyethylene (HDPE) that was shown in Fig. 1C.

**Surface wettability**

The measured water contact angle of the scaffold was 63.839° (Fig. 1E). Since this value is below 90°, the scaffold surface can be considered hydrophilic. This level of wettability may support cell attachment and culture by facilitating initial interactions between the aqueous culture medium and the scaffold surface.

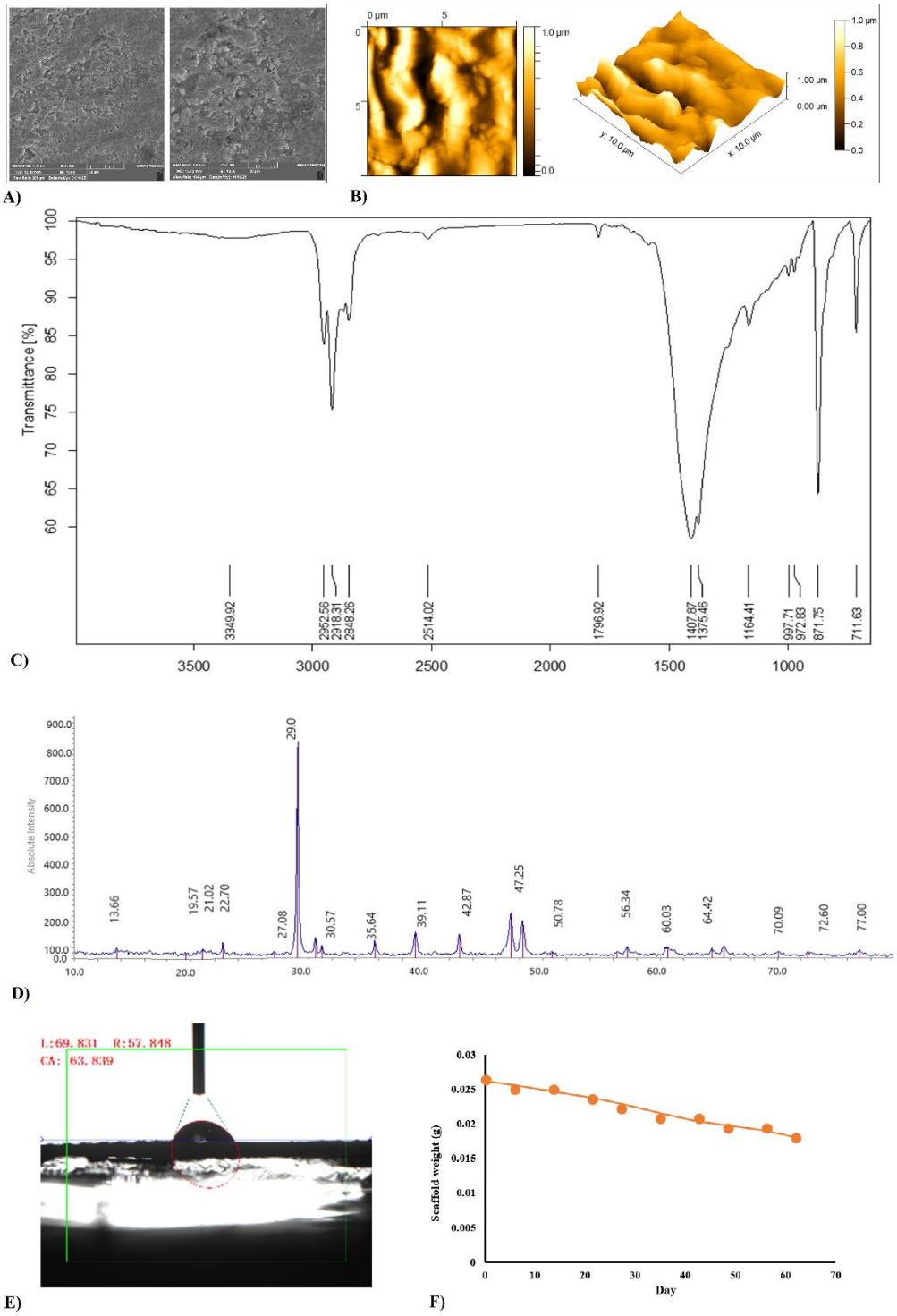


**Fig. 1.** Physicochemical characterization of the mineral paper scaffold: A) SEM micrographs showing a compact and non-uniform surface morphology with limited visible porosity and irregular surface features; B) Two-dimensional and three-dimensional AFM images reveal microscale surface roughness and topographical heterogeneity with peak heights reaching approximately 1 µm; C) FTIR spectrum showing characteristic carbonate absorption bands at 711-877 $cm^{-1}$ and 1375-1407 $cm^{-1}$, as well as C-H stretching vibrations at 2848-2952 $cm^{-1}$; D) XRD pattern confirming calcite as the dominant crystalline phase of calcium carbonate, with the major diffraction peak located at approximately 2θ= 29.0°; E) Water contact angle measurement demonstrating hydrophilic surface behavior with a contact angle of 63.839°; F) *In vitro* degradation profile showing gradual scaffold mass loss in PBS, reaching 30.92% after 62 days of incubation.

### XRD analysis of crystalline structure

Figure 1D illustrates the XRD pattern of the scaffold. The diffraction peaks observed at approximately 2θ= 29.0°, 35.6°, 39.1°, 47.2°, and 60.6° are consistent with the characteristic reflections of calcite $CaCO_3$. The intense peak near 29.0° corresponds to the dominant (104) plane, indicating that calcite is the major crystalline phase in the scaffold. Minor peaks observed at approximately 27.2° and 30.5° may be associated with the aragonite polymorph of $CaCO_3$. Overall, the XRD results suggest that calcite is the dominant crystalline phase, while aragonite may be present as a minor phase

### *In vitro* degradation assessment analysis

The *in vitro* degradation behavior of the scaffold was evaluated by monitoring weight loss during incubation in PBS for 62 days. The scaffold exhibited a gradual decrease in dry weight over time, reaching a total weight loss of 30.92% by day 62. This result indicates moderate degradation (Fig. 1F).

### Phenotypic characterization of ADSCs

Flow cytometry analysis showed high positivity for CD90, CD105, and CD29, with expression levels ranging from 99% to 100%. In contrast, the hematopoietic markers CD34 and CD45 showed low expression levels of 0.6% and 0.5%, respectively. This marker profile is consistent with the expected immunophenotype of mesenchymal stem cells and supports the characterization of ADSCs (Fig. 2).

### Cell viability assessment

The resazurin assay showed a gradual increase in the metabolic activity of ADSCs cultured on the scaffold from day 1 to day 7 ($p< 0.0001$). The absorbance values increased from 0.790 on day 1 to 1.603 on day 7, suggesting that the scaffold supported cell viability and proliferation over time. The higher variability observed on day 7 may be related to uneven cell distribution within the scaffold structure (Fig. 3A).

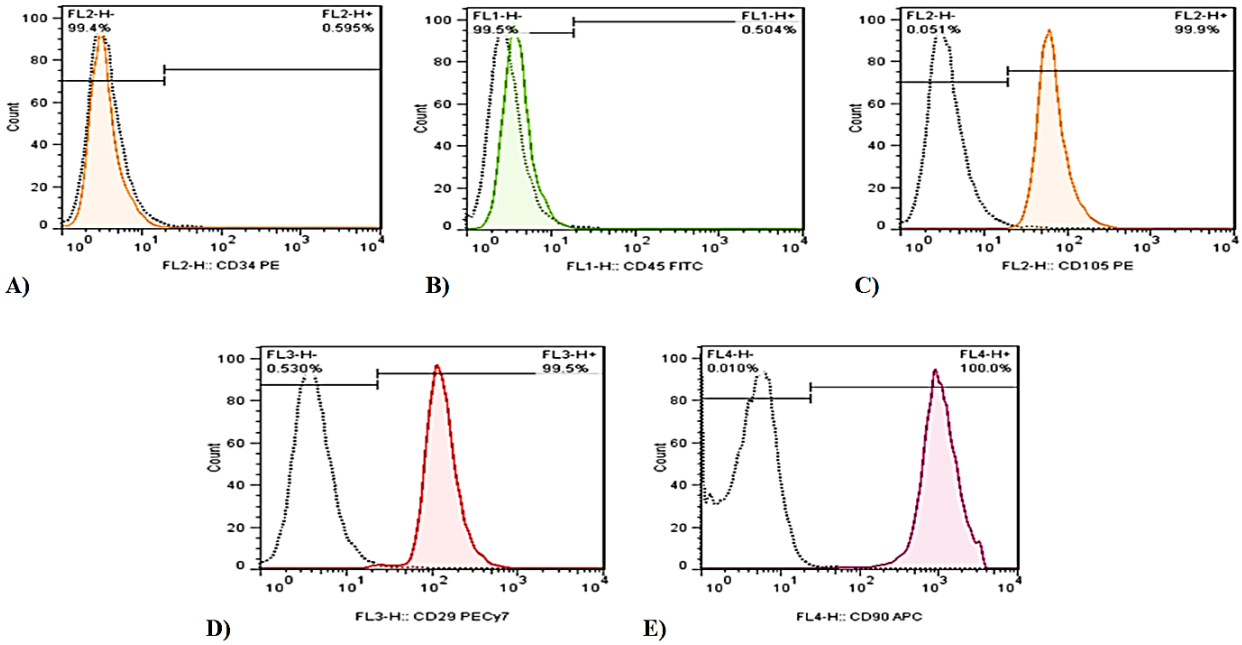


**Fig. 2.** Flow cytometric characterization of adipose-derived mesenchymal stem cells (ADSCs): A) Representative histogram showing the expression of hematopoietic marker CD34; B) Representative histogram showing the expression of hematopoietic marker CD45; C) Representative histogram showing the expression of mesenchymal stem cell marker CD105; D) Representative histogram showing the expression of mesenchymal stem cell marker CD29; E) Representative histogram showing the expression of mesenchymal stem cell marker CD90. ADSCs exhibited high expression of CD90 (100%), CD29 (99.5%), and CD105 (99.9%), together with low expression of CD34 (0.5%) and CD45 (0.5%), confirming their mesenchymal stem cell phenotype according to established criteria.

### ALP activity assay

ALP activity was measured to evaluate the effect of the mineral paper scaffold on the osteogenic potential of ADSCs after 7 and 14 days of culture (Fig. 3B). After seven days, ADSCs cultured on the mineral paper scaffold showed significantly higher ALP activity than those cultured on TCPS ($p<0.01$), with values of approximately 65 U/L and 38 U/L, respectively. A similar trend was observed on day 14, where ALP activity increased to approximately 85 U/L in the scaffold group and 60 U/L in the TCPS group ($p< 0.01$).

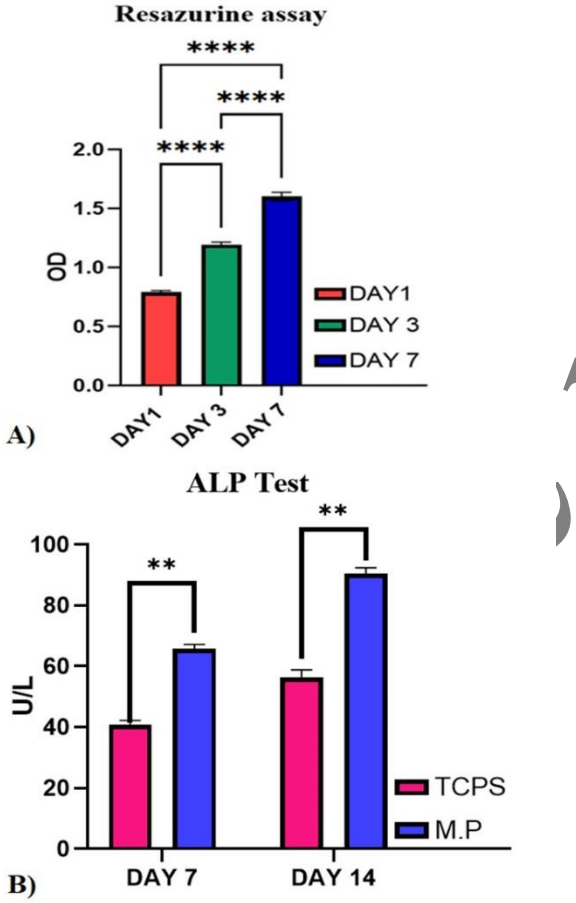


**Fig. 3.** Biological evaluation of ADSCs cultured on the mineral paper scaffold: A) Cell viability assessed by the resazurin assay on days 1, 3, and 7, showing a progressive increase in metabolic activity over time; B) ALP activity of ADSCs cultured on mineral paper (M.P.) and tissue culture polystyrene (TCPS) after 7 and 14 days of osteogenic induction, demonstrating enhanced osteogenic activity in the scaffold group. Data are presented as mean ± SD. Statistical significance is indicated by asterisks (*$p< 0.05$, **$p< 0.01$, ****$p< 0.0001$).

To ensure that the observed increase in ALP activity was specifically due to osteogenic differentiation and not influenced by variations in cell density, cell metabolic activity was monitored using the Resazurin assay. Results indicated comparable metabolic activity across all groups at the time of ALP measurement, confirming that the enhanced ALP activity reflects a higher degree of differentiation rather than differences in cell number. These results suggest that the mineral paper-based scaffold enhanced early osteogenic activity in ADSCs compared with standard TCPS culture.

### ADSC morphology and attachment on the scaffold

SEM micrographs confirmed the successful attachment of ADSCs to the mineral paper scaffold after osteogenic induction (Fig. 4). At day 7, cells exhibited a flattened morphology with visible cytoplasmic extensions anchoring to the scaffold surface, suggesting favorable cell adhesion and spreading. Cell bodies appeared well integrated with the underlying substrate and established multiple contact points with the scaffold. At day 14, attached cells remained detectable on the scaffold surface and continued to exhibit elongated cellular projections. These findings indicate that the mineral paper scaffold provided a suitable surface for maintaining cell attachment during the differentiation period.

### Gene expression analysis

Gene expression analysis was performed on day 14 to evaluate the osteogenic differentiation of ADSCs cultured on the mineral paper scaffold (Fig. 5). Three experimental groups were analyzed: ADSCs cultured on the scaffold, ADSCs cultured on tissue culture polystyrene (TCPS) as the negative control, and mature osteoblasts as the positive control. Relative gene expression levels were calculated using the $2^{-\Delta\Delta Ct}$ method and normalized to *GAPDH*, with the negative control group used as the reference. *RUNX2*, an early osteogenic transcription factor, was significantly upregulated in the scaffold group, showing a 6.68-fold increase compared with the negative control ($p< 0.01$). As expected, the positive control group showed a much higher *RUNX2* expression level, with a 131.6-fold increase.

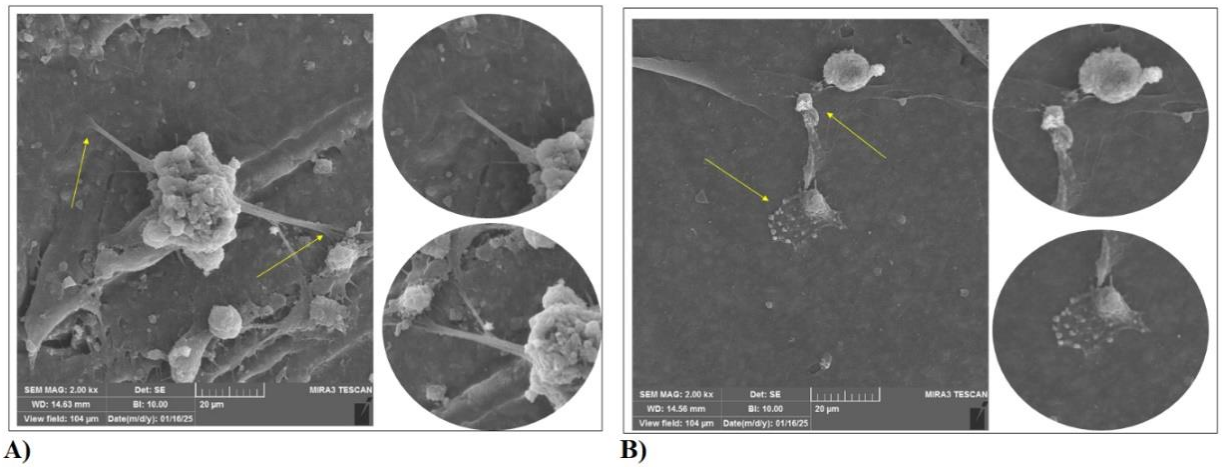


**Fig. 4.** SEM images of ADSCs cultured on the mineral paper scaffold after osteogenic induction, showing cell attachment and spreading on the scaffold surface: A) Day 7; B) Day 14. Images were acquired at ×2.00k magnification. Scale bars = 20 µm.

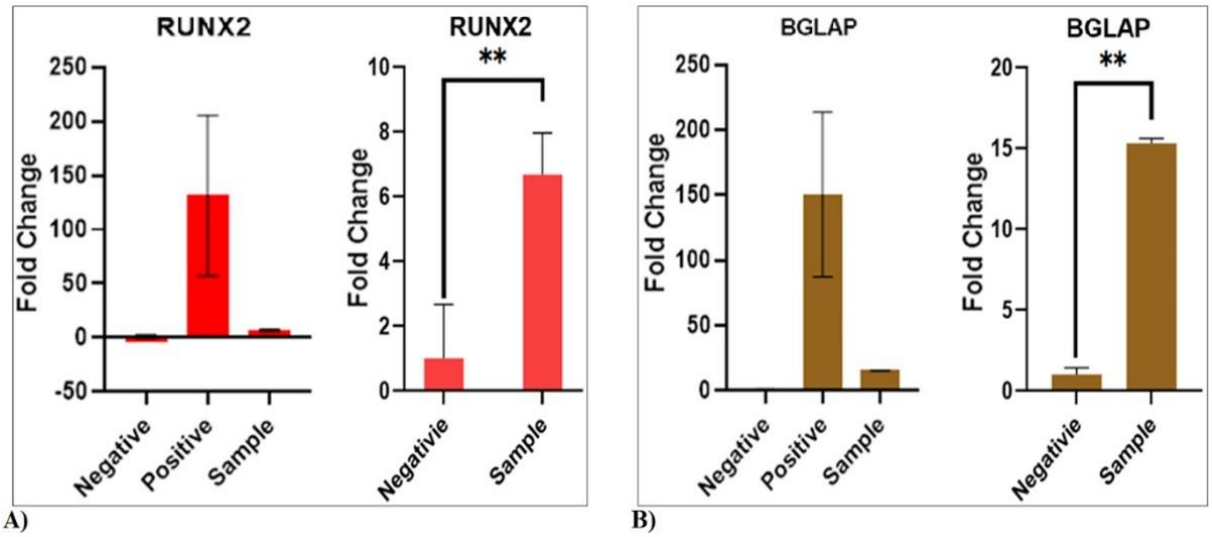


**Fig. 5.** Gene expression analysis of osteogenic markers in ADSCs cultured on the mineral paper scaffold after 14 days of osteogenic induction: A) *RUNX2* expression levels; B) *BGLAP* expression levels. The left panels show relative gene expression in the negative control (TCPS), positive control (mature osteoblasts), and scaffold groups, whereas the right panels show a direct comparison between the scaffold and negative control groups. *RUNX2* expression was increased 6.68- fold in the scaffold group and 131.6- fold in the positive control group relative to the negative control. *BGLAP* expression was increased 15.31- fold in the scaffold group and 150.47- fold in the positive control group relative to the negative control. Data are presented as mean ± SD. **p < 0.01.

*BGLAP*, also known as osteocalcin and commonly associated with late osteogenic differentiation, was also significantly upregulated in the scaffold group. *BGLAP* expression increased by 15.31- fold in the scaffold group (p< 0.01), while the positive control group showed a 150.47-fold increase compared with the negative control. Overall, the increased expression of both *RUNX2* and *BGLAP* indicates that the mineral paper scaffold supported the osteogenic differentiation of ADSCs. However, the lower expression levels compared with mature osteoblasts suggest that the cells had not reached a fully mature osteoblastic phenotype by day 14.

## Discussion

Stem cell-niche interactions depend largely on the physicochemical properties of the material. Surface texture, hydrophilicity, chemical composition, and degradation rate can regulate

cell function through both biochemical and mechanotransduction pathways. For the mineral paper scaffold, this included calcite mineral content, low-moderate hydrophilicity, microscale roughness, and a steady degradation rate, which together supported ADSC viability and osteogenic commitment. Our data confirmed that these factors synergistically formed a suitable microenvironment for osteoinduction without additional inducers. The mineral paper showed a dense heterogeneous surface with microscale protrusions reaching approximately 1 µm height. Surface topography is a key factor affecting cell-material interaction. It directly regulates protein adhesion, focal contact formation, actin skeleton organization, and downstream signaling pathways that determine stem cell fate (Wang *et al*., 2024). Previous studies have shown that microscale roughness increases adsorption of extracellular matrix proteins such as fibronectin and vitronectin, leading to improved cell attachment and spreading mediated by integrins. Upon integrin engagement, mesenchymal stem cells activate mechanotransduction pathways including focal adhesion kinase, PI3K/AKT, and YAP/TAZ signaling (Katoh, 2025). These pathways promote osteogenic commitment, resulting in increased expression of osteogenic markers such as RUNX2 and osteocalcin (Zheng *et al*., 2020; Zou *et al*., 2026). Therefore, the microstructured surface of the mineral paper scaffold likely contributed to the increased ALP activity and osteogenic gene expression observed in this study.

Although the scaffold exhibited favorable surface properties including microscale roughness and hydrophilicity, it lacked interconnected porosity and a true three-dimensional architecture. Scaffold porosity, pore size, and pore interconnectivity are key design parameters in bone tissue engineering, as they govern cell infiltration and migration, support vascularization, facilitate oxygen and nutrient transport, and enable removal of metabolic waste products (Zadpoor, 2015). Recent literature indicates that specific pore size ranges are required to optimize these functions. Smaller pores between 50 and 100 µm foster initial cell attachment, while larger interconnected pores between 200 and 400 µm enhance nutrient diffusion and angiogenesis (Mukasheva *et al*., 2024). The mineral paper provided favorable surface cues for osteogenesis, but its dense architecture prevented ADSC infiltration into deeper regions. This restricts its effectiveness for bulk defect repair when compared with highly porous bone substitutes (Galefi *et al*., 2025; Mandal *et al*., 2021). Future designs could overcome this limitation by introducing porosity through mechanical micro-perforation (Madrid *et al*., 2019), 3D structuring (Toosi *et al*., 2024), or salt-leaching (Bhushan *et al*., 2022) to generate a controlled, interconnected pore network. Given its current compact morphology, mineral paper may be more realistically positioned as a mineral-rich barrier membrane for guided bone regeneration or as a surface coating for implants, where a non-porous structure can prevent soft-tissue invasion while still providing osteoconductive cues to support bone formation at the defect site.

A water contact angle value close to 64 degrees indicated moderate hydrophilicity of the surface. Hydrophilicity is crucial for protein adsorption and cell attachment efficiency. Mesenchymal stem cells demonstrate maximal attachment and spreading on moderately hydrophilic surfaces with contact angles between 40 and 90 degrees, whereas highly hydrophobic surfaces reduce attachment efficiency (Dadashi Oranj *et al.*, 2024). Accordingly, the moderate hydrophilicity of the mineral paper scaffold may promote positive cell-surface interaction and contribute to the observed sustained viability and osteogenic activity of ADSCs. FTIR and XRD results confirmed that calcium carbonate existed in the form of calcite crystals. Calcium carbonate-based materials have gained widespread popularity due to their excellent biocompatibility, osteoconduction capacity, and close chemical composition to the mineral phase of bone (Monchau *et al*., 2013; Woldetsadik *et al*., 2017). Another feature of the scaffold was the presence of high-density polyethylene as a binding component. Nevertheless, the higher abundance of calcium carbonate minimizes the impact of HDPE on hydrophilicity and the ability to support cell attachment and osteogenic activity (Xu *et al*., 2021). Unlike other scaffolds made from calcium phosphate or hydroxyapatite, mineral paper provides an easily affordable source of calcium that requires no preparation. Calcium ion release

has been suggested as one mechanism underlying the bioactivity of calcium carbonate-based biomaterials (Manhas *et al*., 2017; Seol *et al*., 2014). A limitation of this study is the lack of quantitative data on calcium ion release from the mineral paper scaffold during degradation. While the high calcium carbonate content of the scaffold implies potential for ion release, frequently cited as a driver for osteogenic differentiation, our current focus was restricted to assessing macroscopic structural integrity and surface morphology. Consequently, the contribution of released calcium ions versus the influence of the scaffold's intrinsic micro-topography on MSC differentiation remains to be decoupled. Future investigations will employ precise quantification techniques such as inductively coupled plasma optical emission spectrometry to determine dissolution kinetics and their specific correlation with the observed osteogenic response.

The mineral paper-based scaffold lost nearly 31 percent of its mass over 62 days, an intermediate loss rate compared with earlier studies using similar minerals (Xu *et al*., 2021). While the degradation study extended to 62 days to confirm long-term stability, the biological evaluation focused on the first 14 days to capture initial stages of osteogenic commitment. The degradation data revealed that the scaffold maintained over 90 percent of its initial mass during the 14-day biological window. This high structural stability ensures that ADSC attachment and differentiation were mediated by the scaffold's intrinsic surface cues and mineral content, without being confounded by rapid structural breakdown or excessive degradation byproduct release. Metabolic activity analysis using the resazurin assay showed no decline over the seven-day experimental period, suggesting that the mineral paper scaffold did not exert a detectable cytotoxic effect during early culture. The variability observed at certain time points may be attributed in part to heterogeneous distribution of cells on the scaffold surface rather than to loss of cell viability. This observation aligns with previous reports indicating that calcium carbonate-based polymeric matrices can exhibit acceptable biocompatibility and limited adverse biological responses (Arpornmaeklong *et al*., 2023). The favorable metabolic activity observed may relate to the combined influence of high calcium carbonate content, moderate hydrophilicity, and microscale surface topography; however, the relative contribution of each factor remains to be determined. The resazurin assay was performed at days 1, 3, and 7, allowing assessment of initial cell attachment and early metabolic activity on the scaffold. Although additional time points would provide a more comprehensive characterization of proliferation kinetics and possible long-term saturation trends, extending the assay beyond 7 days was not feasible within current time and budget constraints. Future studies should include longer time-course analyses to better define sustained proliferation, long-term viability, and maturation behavior of cells on mineral paper-based scaffolds.

The mineral paper scaffold enhanced osteogenic commitment and differentiation of ADSCs. ALP is traditionally recognized as one of the most common osteogenic markers expressed by committed osteoblasts (Hoemann *et al*., 2009). Higher ALP activity on the mineral paper scaffold at both days 7 and 14 compared with control cells on TCPS indicates scaffold-induced enhancement of osteogenesis, similar to previous reports on calcium carbonate-based scaffolds showing increased expression of genes responsible for osteogenic processes such as ALP activity and collagen secretion (Li *et al*., 2018). The mineral paper scaffold upregulated two key osteogenic markers, RUNX2, a transcription factor that drives osteoblast commitment, and BGLAP (osteocalcin), which is associated with matrix maturation and late stages of osteogenesis. This profile indicates that ADSCs cultured on mineral paper entered the osteogenic differentiation pathway, consistent with previous observations on calcium carbonate-based substrates (Liu and Wang, 2023). However, the magnitude of osteogenic induction on mineral paper was lower than that reported for more advanced calcium carbonate-based composite systems incorporating additional organic or inorganic components or bioactive cues (Bao *et al*., 2020), and direct comparison should therefore be interpreted with caution. Although RUNX2 and BGLAP expression in ADSCs on mineral paper remained below the levels measured in mature osteoblasts, this does not necessarily preclude functional relevance for bone tissue engineering

applications. The literature supports that stem cells or early mesenchymal progenitors are more suitable for cell-based regeneration than differentiated cells, which not only lose proliferative and differentiation capacity upon expansion but also require invasive tissue retrieval (Hasanzadeh *et al*., 2024). In this context, the goal of the scaffold is not to drive complete in vitro maturation to a fully osteoblast-like phenotype but rather to promote osteogenic commitment to a pre-osteogenic state that can undergo further maturation in vivo under the influence of the physiological microenvironment, mechanical loading, and host-derived factors. The upregulation of osteogenic markers on mineral paper is clinically meaningful. Implanting partially differentiated stem cells on scaffolds is a well-established approach that supports construct integration and in vivo maturation without requiring full differentiation beforehand. Mineral paper therefore directs ADSCs toward osteogenic commitment, a necessary step for bone formation *in vivo*.

## Conclusion

Mineral paper sustained ADSCs attachment and drove osteogenic differentiation. The scaffold exhibited a primary calcite mineral phase, moderate hydrophilicity, and microscale surface roughness, features known to influence cell adhesion and differentiation, along with gradual degradation over the 62-day culture period. The moderate hydrophilicity promoted cell attachment, while the surface roughness provided topographical cues for osteogenic commitment. The degradation rate aligned with bone healing timelines, indicating favorable biocompatibility. The scaffold significantly elevated ALP activity, while cells on mineral paper-based scaffold exhibited a progressive increase in osteogenic gene expression (RUNX2 and BGLAP) relative to the control group. Remarkably, differentiation occurred without any exogenous osteogenic supplements or growth factors, underscoring the intrinsic osteoconductive potential of the calcium-rich substrate. Although the osteogenic response remained below that of mature osteoblasts, the scaffold directed ADSCs through both early and late differentiation stages. Overall, mineral paper offers a simple, low-cost, calcium-based scaffold for bone repair. However, calcium ion release, long-term matrix mineralization, mechanical performance during degradation, and *in vivo* bone regeneration require further investigation before clinical translation.

## Acknowledgments

The authors would like to thank Dr. Zeinab Shirvani Farsani for her insightful helps and discussions.

## Conflict of interests

The authors declare no conflict of interest.

## Declaration of generative AI and AI-assisted technologies in the manuscript preparation process

During the preparation of this manuscript, the authors utilized ChatGPT (GPT-4o) for grammatical and typographical editing. The authors subsequently reviewed and refined the content and accept full responsibility for the final published text.

## References

Alvarez, K., & Nakajima, H. (2009). Metallic scaffolds for bone regeneration. *Materials*, 2(3), 790-832. https://doi.org/10.3390/ma2030790

Arpornmaeklong, P., Jaiman, N., Apinyauppatham, K., Fuongfuchat, A., & Boonyuen, S. (2023). Effects of calcium carbonate microcapsules and nanohydroxyapatite on properties of thermosensitive chitosan/collagen hydrogels. *Polymers*, 15(2), 416. https://doi.org/10.3390/polym15020416

Bao, Z., Gu, Z., Xu, J., Zhao, M., Liu, G., & Wu, J. (2020). Acid-responsive composite hydrogel platform with space-controllable stiffness and calcium supply for enhanced bone regeneration. *Chemical Engineering Journal*, 396, 125353. https://doi.org/10.1016/j.cej.2020.125353

Battafarano, G., Rossi, M., De Martino, V., Marampon, F., Borro, L., Secinaro, A., & Del Fattore, A. (2021). Strategies for bone regeneration: from graft to tissue engineering. *International Journal of Molecular Sciences*, 22(3), 1128. https://doi.org/10.3390/ijms22031128

Bhushan, S., Singh, S., Maiti, T. K., Sharma, C., Dutt, D., Sharma, S., Li, C., & Tag Eldin, E. M. (2022). Scaffold fabrication techniques of biomaterials for bone tissue engineering: A critical review. *Bioengineering*, 9(12), 728. https://doi.org/10.3390/bioengineering9120728

Chernozem, R. V., Surmeneva, M. A., Shkarina, S. N., Loza, K., Epple, M., Ulbricht, M., ... & Surmenev, R. A. (2019). Piezoelectric 3-D fibrous poly (3-hydroxybutyrate)-based scaffolds ultrasound-mineralized with calcium carbonate for bone tissue engineering: inorganic phase formation, osteoblast cell adhesion, and proliferation. *American Chemical Society Applied Materials and Interfaces*, 11(21), 19522-19533. https://doi.org/10.1021/acsami.9b04936

Chu, C., & Nel, P. (2019). Characterisation and deterioration of mineral papers. *Australian International Composite Conference and Materials*, 40(1), 37-49. https://doi.org/10.1080/10344233.2019.1672951

Ciancia, S., Holer, W., Sakkers, R., Appelman-Dijkstra, N., Boot, A., Sas, T., & Renes, J. (2022). Osteoporosis in children and adolescents: How to treat and monitor? *European Journal of Pediatrics*, 182, 501-511. https://doi.org/10.1007/s00431-022-04743-x

Dadashi Oranj, Z., Hosseini, S., Alipour, A., Homaeigohar, S., Azari, S., Ghazizadeh, L., Shokrgozar, M., Thomas, S., Irian, S., & Shahsavarani, H. (2024). The potent osteo-inductive capacity of bioinspired brown seaweed-derived carbohydrate nanofibrous three-dimensional scaffolds. *Marine Life Science and Technology*, 6, 515-534. https://doi.org/10.1007/s42995-024-00241-1

De Pace, R., Molinari, S., Mazzoni, E., & Perale, G. (2025). Bone regeneration: A review of current treatment strategies. *Journal of Clinical Medicine*, 14(6). https://doi.org/10.3390/jcm14061838

Donnaloja, F., Jacchetti, E., Soncini, M., & Raimondi, M. (2020). Natural and synthetic polymers for bone scaffolds optimization. *Polymers*, 12(4), 905. https://doi.org/10.3390/polym12040905

Duda, G., Geissler, S., Checa, S., Tsitsilonis, S., Petersen, A., & Schmidt-Bleek, K. (2023). The decisive early phase of bone regeneration. *Nature Reviews Rheumatology*, 19, 78-95. https://doi.org/10.1038/s41584-022-00887-0

Farjaminejad, S., Farjaminejad, R., Hasani, M., Garcia-Godoy, F., Abdouss, M., Marya, A., Harsoputranto, A., & Jamilian, A. (2024). Advances and challenges in polymer-based scaffolds for bone tissue engineering: A path towards personalized regenerative medicine. *Polymers*, 16(23). https://doi.org/10.3390/polym16233303

Ferraz, M. P. (2023). Bone grafts in dental medicine: an overview of autografts, allografts and synthetic materials. *Materials*, 16(11), 4117. https://doi.org/10.3390/ma16114117

Ferraz, M. P. (2024). An overview on the big players in bone tissue engineering: biomaterials, scaffolds and cells. *International Journal of Molecular Sciences*, 25(7), 3836. https://doi.org/10.3390/ijms25073836

Filippi, M., Born, G., Chaaban, M., & Scherberich, A. (2020). Natural polymeric scaffolds in bone regeneration. *Frontiers in Bioengineering and Biotechnology*, *8*, 474. https://doi.org/10.3389/fbioe.2020.00474

Galefi, A., Hosseini, S., Alipour, A., Banaeyan, R., Farrokhi, N., Amanzadeh, A., Wang, P.Y., Zarrabi, A., Shahsavarani, H., & Jahanfar, M. (2025). Synergistic enhancement of osteogenesis: silica nanoparticles and proanthocyanidin on bioinspired nanofibrous scaffolds for craniofacial bone regeneration. *Emergent Materials*, 8, 2575-2598. https://doi.org/10.1007/s42247-024-00909-5

Hajihassani, H., Farrokhi, N., Rezazadeh, A., Aligol, M.S., & Shahsavarani, H. (2026). Sustainable multimodal platforms for bone regeneration: Bridging the translational gap with bioinspired natural materials. *Sustainable Materials and Technologies*, 49, e02102. https://doi.org/10.1016/j.susmat.2026.e02102

Hakami, I. A. (2024). An outline on the advancements in surgical management of osteoporosis-associated fractures. *Cureus*, *16*(6). https://doi.org/10.7759/cureus.63226

Hasanzadeh, A., Alipour, A., Ghasemi, S., Hosseini, S., Farrokhi, N., Wang, P.Y., ... & Shahsavarani, H. (2024). Proanthocyanidin-imbued cellulosic 3-dimensional intrinsic aligned nanostructures: A novel approach for dental and bone regeneration using dental pulp derived stem cells. *Journal of Science: Advanced Materials*

*and Devices*, 9(4), 100820. https://doi.org/10.1016/j.jsamd.2024.100820

Hoemann, C., El-Gabalawy, H., & McKee, M. (2009). *In vitro* osteogenesis assays: influence of the primary cell source on alkaline phosphatase activity and mineralization. Pathologie *Biologie*, 57(4), 318-323. https://doi.org/10.1016/j.patbio.2008.06.004

Jeong, J., Kim, J. H., Shim, J. H., Hwang, N. S., & Heo, C. Y. (2019). Bioactive calcium phosphate materials and applications in bone regeneration. *Biomaterials Research*, 23(1), 4. https://doi.org/10.1186/s40824-018-0149-3

Kajander, K., Sirkia, S., Vallittu, P., Heino, T., & Maatta, J. (2023). Bioactive glasses promote rapid pre-osteoblastic cell migration in contrast to hydroxyapatite, while carbonated apatite shows migration inhibiting properties. *Scientific Reports*, 13(1), 20587. https://doi.org/10.1038/s41598-023-47883-2

Katoh, K. (2025). Integrin and its associated proteins as a mediator for mechano-signal transduction. *Biomolecules*, 15(2), 166. https://doi.org/10.3390/biom15020166

Kotsifaki, A., Kalouda, G., Maroulaki, S., Foukas, A., & Armakolas, A. (2025). The genetic and biological basis of pseudoarthrosis in fractures: current understanding and future directions. *Diseases*, 13(3), 75. https://doi.org/10.3390/diseases13030075

Li, X., Yang, X., Liu, X., He, W., Huang, Q., Li, S., & Feng, Q. (2018). Calcium carbonate nanoparticles promote osteogenesis compared to adipogenesis in human bone-marrow mesenchymal stem cells. *Progress in Natural Science: Materials International*, 28(5), 598-608. https://doi.org/10.1016/j.pnsc.2018.09.004

Liu, J., Yang, L., Liu, K., & Gao, F. (2023). Hydrogel scaffolds in bone regeneration: Their promising roles in angiogenesis. *Frontiers in Pharmacology*, 14, 1050954. https://doi.org/10.3389/fphar.2023.1050954

Liu, X., & Ma, P. X. (2004). Polymeric scaffolds for bone tissue engineering. *Annals of Biomedical Engineering*, 32(3), 477-486. https://doi.org/10.1023/B:ABME.0000017544.36001.8e

Liu, X., & Wang, Z. (2023). Chitosan-calcium carbonate scaffold with high mineral content and hierarchical structure for bone regeneration. *Smart Materials in Medicine*, 4, 552-561. https://doi.org/10.1016/j.smaim.2023.04.004

Livak, K. J., & Schmittgen, T. D. (2001). Analysis of relative gene expression data using real-time quantitative PCR and the $2^{-\Delta\Delta CT}$ method. *Methods*, 25(4), 402-408. https://doi.org/10.1006/meth.2001.1262

Madrid, A. P. M., Vrech, S. M., Sanchez, M. A., & Rodriguez, A. P. (2019). Advances in additive manufacturing for bone tissue engineering scaffolds. *Materials Science and Engineering*, 100, 631-644. https://doi.org/10.1016/j.msec.2019.03.037

Mandal, S., Nandi, S. K., & Roy, M. (2021). Effects of multiscale porosity and pore interconnectivity on *in vitro* and *in vivo* degradation and biocompatibility of Fe-Mn-Cu scaffolds. *Journal of Materials Chemistry*, 9(21), 4340-4354. https://doi.org/10.1039/D1TB00641J

Manhas, V., Guyot, Y., Kerckhofs, G., Chai, Y. C., & Geris, L. (2017). Computational modelling of local calcium ions release from calcium phosphate-based scaffolds. *Biomechanics and Modeling in Mechanobiology*, 16(2), 425-438. https://doi.org/10.1007/s10237-016-0827-9

Min, K., Kim, D. H., Kim, K. H., Seo, J.-H., & Pack, S. P. (2024). Biomimetic scaffolds of calcium-based materials for bone regeneration. *Biomimetics*, 9(9), 511. https://doi.org/10.3390/biomimetics9090511

Monchau, F., Hivart, P., Genestie, B., Chai, F., Descamps, M., & Hildebrand, H. (2013). Calcite as a bone substitute, Comparison with hydroxyapatite and tricalcium phosphate with regard to the osteoblastic activity. *Materials Science and Engineering*, 33(1), 490-498. https://doi.org/10.1016/j.msec.2012.09.019

Moy, J., Limaye, A., & Arinzeh, T. L. (2020). Fibrous scaffolds for bone tissue engineering. *Artificial Protein and Peptide Nanofibers*, 351-382. https://doi.org/10.1016/B978-0-08-102850-6.00015-2

Mukasheva, F., Adilova, L., Dyussenbinov, A., Yernaimanova, B., Abilev, M., & Akilbekova, D. (2024). Optimizing scaffold pore size for tissue engineering: insights across various tissue types. *Frontiers in Bioengineering and Biotechnology*, 12, 1444986. https://doi.org/10.3389/fbioe.2024.1444986

Qi, J., Yu, T., Hu, B., Wu, H., & Ouyang, H. (2021). Current biomaterial-based bone tissue engineering and translational medicine. *International Journal of Molecular Sciences*, 22(19), 10233. https://doi.org/10.3390/ijms221910233

Ribas, R., Schatkoski, V., Montanheiro, T., Menezes, B., Stegemann, C., Leite, D., & Thim, G. (2019). Current advances in bone tissue engineering concerning ceramic and bioglass scaffolds: A review. *Ceramics International*, 45(17), 21051-21061. https://doi.org/10.1016/j.ceramint.2019.07.096

Schulze, F., Lang, A., Schoon, J., Wassilew, G., & Reichert, J. (2023). Scaffold guided bone regeneration for the treatment of large segmental defects in long bones. biomedicines, *Biomedicines*, 11(2), 325. https://doi.org/10.3390/biomedicines11020325

Seol, Y.J., Park, J. Y., Jung, J. W., Jang, J., Girdhari, R., Kim, S. W., & Cho, D.W. (2014). Improvement of bone regeneration capability of ceramic scaffolds by accelerated release of their calcium ions. *Tissue Engineering*, 20(21-22), 2840-2849. https://doi.org/10.1089/ten.TEA.2012.0726

Toosi, S., Javid-Naderi, M. J., Tamayol, A., Ebrahimzadeh, M. H., Yaghoubian, S., & Mousavi Shaegh, S. A. (2024). Additively manufactured porous scaffolds by design for treatment of bone defects. *Frontiers in Bioengineering and Biotechnology*, 11, 1252636. https://doi.org/10.3389/fbioe.2023.1252636

Wang, M. (2006). Composite scaffolds for bone tissue engineering. *American Journal of Biochemistry and Biotechnology*, 2(2), 80-84. http://dx.doi.org/10.3844/ajbbsp.2006.80.84

Wang, P.Y., Shahsavarani, H., Chen, H.Y., & Dalby, M.J. (2024). Editorial: Harnessing biomechanotransduction to influence cell fate. *Frontiers in Bioengineering and Biotechnology*, 11, 1357961. https://doi.org/10.3389/fbioe.2023.1357961

Wen, Y., Xun, S., Haoye, M., Baichuan, S., Peng, C., Xuejian, L., Kaihong, Z., Xuan, Y., Jiang, P., & Shibi, L. (2017). 3D printed porous ceramic scaffolds for bone tissue engineering: A review. *Biomaterials Science*, 5(9), 1690-1698. https://doi.org/10.1039/c7bm00315c

Woldetsadik, A., Sharma, S., Khapli, S., Jagannathan, R., & Magzoub, M. (2017). Hierarchically porous calcium c Scaffolds for bone tissue engineering. *American Chemical Society Biomaterials Science and Engineering*, 3(10), 2457-2469. https://doi.org/10.1021/acsbiomaterials.7b00301

Xu, H. H., Wang, P., Wang, L., Bao, C., Chen, Q., Weir, M. D., ... & Reynolds, M. A. (2017). Calcium phosphate cements for bone engineering and their biological properties. *Bone Research*, 5(1), 17056. https://doi.org/10.1038/boneres.2017.56

Xu, W., Zhao, R., Wu, T., Li, G., Wei, K., & Wang, L. (2021). Biodegradable calcium carbonate/mesoporous silica/poly (lactic-glycolic acid) microspheres scaffolds with osteogenesis ability for bone regeneration. *Royal Society of Chemistry Advances*, 11(9), 5055-5064. https://doi.org/10.1039/d0ra09958a

Younger, E. M., & Chapman, M. W. (1989). Morbidity at bone graft donor sites. *Journal of Orthopaedic Trauma*, 3(3), 192-195. https://doi.org/10.1097/00005131198909000-00002

Zadpoor, A. A. (2015). Bone tissue regeneration: the role of scaffold geometry. *Biomaterials Science*, 3(2), 231-245. https://doi.org/10.1039/c4bm00291a

Zheng, H., Tian, Y., Gao, Q., Yu, Y., Xia, X., Feng, Z., ... & Sui, L. (2020). Hierarchical micro-nano topography promotes cell adhesion and osteogenic differentiation via integrin α2-PI3K-AKT signaling axis. *Frontiers in Bioengineering and Biotechnology*, *8*, 463. https://doi.org/10.3389/fbioe.2020.00463

Zou, Z., Jiang, S., Chen, W., Wang, Y., Liang, Q., Fang, W., Zhan, X., Gu, R., & Chen, Q. (2026). Research on the regulation of osteogenic differentiation and mechanotransduction by porous bionic coatings on titanium alloy implant surfaces. *Royal Society of Chemistry Advances*, 16(23), 21381-21396. https://doi.org/10.1039/d6ra01182a